Korean J. Chem. Eng., 33(5), 1551-1556 (2016)
DOI: 10.1007/s11814-015-0271-z

pISSN: 0256-1115
eISSN: 1975-7220

Trimetallic catalyst synthesized multi-walled carbon nanotubes and their application for hydrogen storage

Sami Ullah Rather†

Department of Chemical and Materials Engineering, King Abdulaziz University, P. O. Box 80204, Jeddah 21589, Saudi Arabia
(*Received 23 November 2014 • accepted 8 December 2015*)

Abstract−Multi-walled carbon nanotubes (MWCNTs) were synthesized by rapid thermal decomposition method using trimetallic catalyst supported MgO. MWCNTs prepared via trimetallic catalyst shows much higher BET specific surface area compared to current monometallic and bimetallic catalyst. As-grown and pristine MWCNTs were found to adsorb nitrogen reversibly and their adsorption uptake exhibits type-II BET isotherm. Existence of small impurities, such as metal and metal oxides present in the MWCNTs, was confirmed by thermogravimetric analysis as well as via energy-dispersive X-ray spectroscopy. An over 10 wt% enhancement of hydrogen storage capacity of as-grown MWCNTs compared to pristine was found to be due to the presence of impurities. Fast kinetics and complete reversibility gives indication that the process responsible for hydrogen adsorption uptake in MWCNTs is physisorption. A linear relation between hydrogen uptake (~0.22 and 0.20 wt%) and equilibrium hydrogen pressure was obtained for both as-grown and pristine MWCNTs.

Keywords: Carbon Nanotube, Physisorption, Decomposition, Trimetallic Catalyst, Chemical Vapor Deposition, Hydrogen Storage

INTRODUCTION

Hydrogen, as a clean and renewable energy carrier, is expected to replace existing fossil fuels in near future, attributable to rapid depletion and severe environmental problems. Hydrogen has one important potential of zero-emission, which makes it a promising fuel for the transportation and stationary applications. A hydrogen economy not only has the potential to reduce the environmental impacts via implementation of zero emission energy devices, but also can effectively resolve the energy security issues associated with the rising energy demands of the present-day world. However, the lack of an efficient, reliable, and affordable medium that can reversibly store hydrogen possesses the most formidable threat to the public acceptance and wider utilization of hydrogen fuel [1,2]. The discovery of carbon nanotubes, both single and multi-walled and their interaction with hydrogen, makes this a reasonable candidate for hydrogen storage. Revised gravimetric and volumetric targets set by the US Department of Energy (DOE) in 2009 for on-board hydrogen uptake systems are 1.5 kWh/kg (4.5 wt%) and 0.9 kWh/L in 2010 and 1.8 kWh/kg (5.5 wt%) and 1.3 kWh/L in 2015. The above set targets proposed by the DOE is based on achieving a driving range of more than 300 miles (500 km) on a single fill for hydrogen powered vehicles [3-10].

Hydrogen can be stored in different forms such as metal hydrides, complex hydrides, intermetallic hydrides, liquefaction, compressed gas, and physisorption [11,12]. Promising hydrogen uptake material is necessary to have a high safety, low dissociation temperature, moderate pressure, fast kinetics, low cost of recycling, reversibility, and charging infrastructure. Following these different forms of hydrogen storage, physisorption is considered as the most attractive and effective phenomenon. Nanoporous activated carbon (AC), single- and multi-walled carbon nanotubes (SWCNTs and MWCNTs), zeolites, and metal-organic frameworks (MOFs) have been proposed as best physisorption materials for storage of hydrogen. SWCNTs and MWCNTs, owing to their unique nanoporous structure, high specific surface area, tunable properties, and low mass density are considered as the prospective solid-state reversible hydrogen storage medium [13-15]. It is well established that hydrogen adsorbs on exterior walls, within the mesoporous tube channels (endohedral), and also in the void regions that exist among individual entangled nanotubes or nanotube bundles [16]. In addition, hydrogen can occupy the interstitial spaces within the 2-D triangular lattices that are formed by the association of large-diameter individual SWCNTs [17]. In MWCNTs, an interesting situation arises when we consider the intercalation of hydrogen between the concentric tubes [18]. The space among the adjacent tube walls of MWCNTs is 0.34 nm, significantly larger than the kinetic diameter of molecular hydrogen (0.289 nm) [19]. Due to its higher heat of adsorption, filling of hydrogen in these micropores contributes significantly to the storage capacity when compared with the adsorption on external walls, particularly at relatively low pressures [20].

In this research work, pristine high surface area synthesized MWCNTs using new trimetallic catalyst (Co-Mo-V) supported on porous magnesium oxide (MgO) and its hydrogen uptake studies are presented. Trimetallic catalyst with support as compared to existing bimetallic and monometallic catalyst furnish fresh idea of improving the surface area of MWCNTs. The hydrogen storage capac-

†To whom correspondence should be addressed.
E-mail: rathersami@gmail.com, rathersami@kau.edu.sa

ity of as grown and pristine MWCNTs was determined by using Sievert's volumetric apparatus at room temperature (RT). Hydrogen storage studies of both as-grown and purified sample shows that the former storing more hydrogen is due to the presence of impurities such as metals or metal oxides in the sample. Linear scaling of hydrogen adsorption uptake was observed for both samples.

EXPERIMENTAL

1. Synthesis of Multi-walled Carbon Nanotubes (MWCNTs)

Cobalt (II) acetate tetrahydrate, ammonium molybdate, vanadium (II) chloride, and magnesium oxide powder were purchased from Sigma Aldrich and used without further purification. MWCNTs were prepared by the catalytic decomposition of acetylene (C_2H_2) over new synthesized Co-Mo-V trimetallic catalyst and porous magnesium oxide (MgO) as a supporter. The rapid thermal chemical vapor deposition (RTCVD) technique has been designed for the growth of MWCNTs. The catalytic weight composition 15Co: 10Mo: 5V: 70MgO was synthesized by the impregnation method. For trimetallic Co-Mo-V/MgO catalysis synthesis, 4.52 g (18.146 mmol) of cobalt (II) acetate tetrahydrate, 1.31 g (1.06 mmol) of ammonium molybdate, and 0.23 g (1.88 mmol) of vanadium (II) chloride were mixed and dissolved in water. The suspension was mixed with 5 g (124.03 mmol) of magnesium oxide powder and vigorously stirred at 80 °C to obtain the slurry. The slurry was dried at 100 °C for 12 h and then calcined at 500 °C for 5 h. For the preparation of MWCNTs, 0.2 g of above synthesized trimetallic catalyst was uniformly dispersed in an alumina boat with a diameter of 3 cm and length 13.9 cm, placed in the central region of a horizontal quartz-tube reactor. Prior to growth of MWCNTs, trimetallic catalyst was activated at 500 °C for 1 hour in a 100-sccm H_2 gas flow. After activation, a mixture of acetylene and hydrogen gas in the volume ratio of 10 : 100 sccm for 30 min was passed at 800 °C to grow MWCNTs and considered as raw MWCNTs.

2. Purification of MWCNTs

To remove support, metal, metal oxide, and amorphous carbon as an impurity from MWCNTs, ultrasonication in deionized (DI) water for 30 minutes at room temperature (RT) was performed. The volume of the suspension was made double by adding 60% HNO_3 and vigorously stirring at 80 °C for 30 min. After 48 h, it was filtered by using normal micro filter paper and washed repeatedly by DI water until the effluent became acid free. The recovered solid was dispersed into DI water again and boiled for 15 min to remove adsorbed anion from acid. The sample was dried overnight in an oven at around 100 °C. The black product obtained after drying was treated in HCl and stirred for 1 hr to remove the metal particles at RT. Finally, the product was washed with DI water, dried and considered as pristine MWCNTs. Characterization of both raw and pristine samples was performed by powder X-ray diffraction (D/MAX 2500 Rigaku, Cu Kα radiation), scanning electron microscopy (Hitachi, S-4700), thermogravimetric analysis (10 °C/min, TGA, TGAQ50), transmission electron microscopy (JEOL JEM-2010), Brunauer-Emmett-Teller N_2 adsorption isotherm techniques (BET, ASAP 2000), Raman spectroscopy (RENISHAW, Microraman spectrometer) enabled with an He-Ne laser line of excitation wavelength 623 nm, and energy dispersive X-ray analysis (EMAX, HORIBA, 10 KeV) technique.

3. Hydrogen Storage of Multi-walled Carbon Nanotubes (MWCNTs)

Hydrogen storage studies of both raw and pure MWCNTs sample was performed at 298 K using Sievert's volumetric equipment. The equipment consists of hydrogen buffer-tank, which was connected to the reactor and a high sensitivity and calibrated pressure transducer (0.05% error at full scale). Entire setup was placed in an isothermal bath, whose temperature was monitored and controlled via proportional-integral-differential (PID) controlled thermostat. Prior to the storage experiments, we determined the dead-volume of the system; it was additionally cross-checked by using hydrogen adsorption data of a known amount of the intermetallic alloy $LaNi_5$ [21]. The overall leak-rate of the system determined using helium gas was found to be negligible. Nearly 0.1 g sample was used in each storage study. Prior to each adsorption experiment, the sample was out-gassed for nearly 6 h by heating to 200 °C under continuous evacuation up to 10^{-4} Torr. The degassing was typically performed until a constant and reproducible background pressure was obtained. For adsorption experiments, high purity hydrogen gas (99.9999%) was admitted into the buffer and maintained until equilibrium was established. Then, the gas was isothermally vented into the reactor and the pressure drop of the hydrogen gas was measured as a function of time. The gravimetric storage capacity of nanostructured sample was determined from the pressure drop of hydrogen gas using ideal gas equation PV=nRT. Additional re-adsorption experiments were performed on previously adsorbed samples after degassing of the samples at 200 °C for nearly 4 h. Data acquisition for hydrogen storage was automated by interfacing the pressure transducer output to a PC via RS-232 device. Further experimental details can be obtained elsewhere [21].

RESULTS AND DISCUSSION

In Fig. 1(a) and (b), a high-angle X-ray diffraction (XRD) pattern of as-grown and pristine MWCNTs prepared by chemical vapor deposition (CVD) using a trimettalic-supported catalyst (Mo-

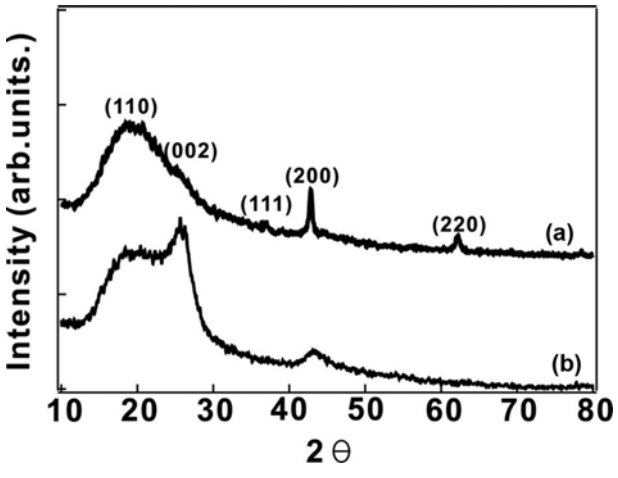

Fig. 1. X-ray diffraction (XRD) pattern of (a) as-grown and (b) purified MWCNTs synthesized via trimetallic Mo-Co-V/MgO catalysts for 30 min at 800 °C under 10/100 sccm C_2H_2/H_2 flow.

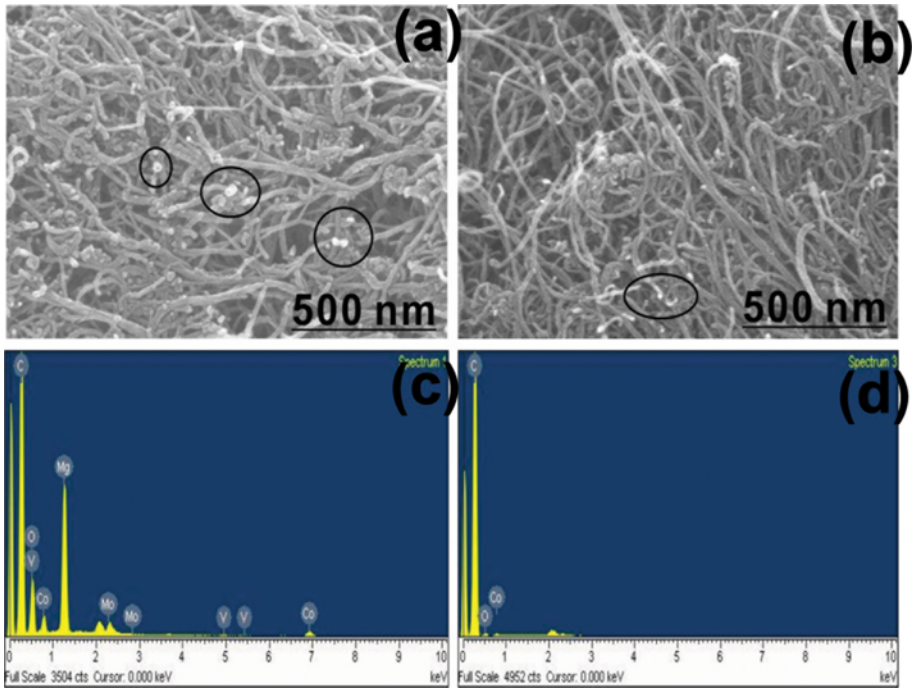

Fig. 2. (a) and (b) are SEM images of as-grown and pristine MWCNTs. (c) and (d) are EDX spectrum of as-grown and pristine MWCNTs.

Co-V/MgO) is displayed. XRD spectra are characterized by several intense peaks between diffraction angle of 10 and 80°. XRD of both raw and pure MWCNTs showed only CNT and MgO peaks. The peaks in spectrum correspond to the reflection of (110), (002), (111), (200), (220) lattice planes of graphite, carbon nanotubes, and magnesium oxide. The (200) peak of pristine MWCNTs displayed in Fig. 1(b) becomes broader as compared to as-grown MWCNTs (a), indicating smaller diameter of nanotubes after acid treatment. The disappearance of (111) and (220) in Fig. 1(b) indicates purity of MWCNTs.

Morphology of as-grown and pristine MWCNTs analyzed by scanning electron microscopy (SEM) is displayed in Fig. 2(a) and (b). White patches seen over the as-grown and pristine MWCNTs are the metal particles lying on the walls of carbon nanotubes. Most of the white patches are seen lying on the tip of the carbon nanotubes, and these patches are denser in the raw samples as compared to pristine. Energy dispersive X-ray (EDX) spectrum of as-grown and pristine MWCNTs is displayed in Fig. 2(c) and (d). EDX spectrum of as grown sample shows more than 74% of carbon and trimetallic-supported catalyst was also present. After purification by 60% HNO_3, almost all impurity present in as-grown sample disappeared, except for a very minute quantity. More appropriate content calculation of the impurities present in both MWCNTs sample was performed by thermogravimetric analysis (TGA). Fig. 3 shows TGA data performed in a lean oxygen atmosphere using a heating ramp of 10 °C/min of as grown and pristine MWCNTs. Here profile (a) corresponds to the TGA data of as-grown MWCNTs and (b) represents the pristine MWCNTs. The single weight loss recorded around ~520 °C corresponds to the combustion of carbon nanotubes. The recorded weight loss for as-grown MWCNTs is related to the impurities such as metal and metal oxides present

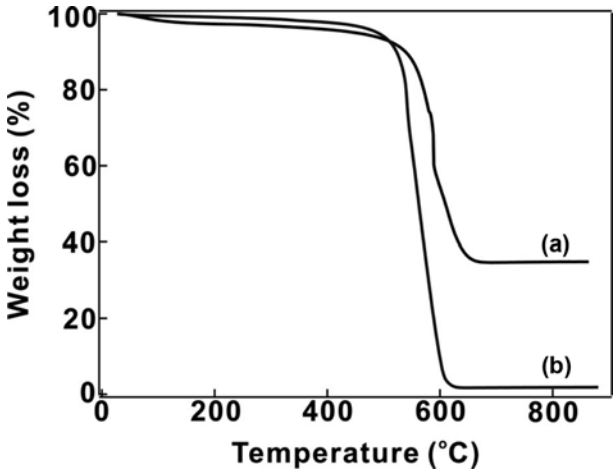

Fig. 3. Thermogravimetric analysis (TGA) of (a) raw (b) pristine MWCNTs prepared by rapid thermal chemical vapor analysis (RTCVD).

in the sample and impurity level was drastically decreased to ~2% post acid treatment of as grown sample. The weight-loss recorded for both as-grown and pristine MWCNTs matches well with EDX data shown in Fig. 2(c) and (d). Transmission electron microscopy (TEM) images of as-grown (a and b) and purified samples (c and d) are shown in Fig. 4. The tube diameter of as-grown and purified MWCNTs is ~4-15 nm and ~8-14 nm, respectively (Table 1).

Fig. 5 (a) and (b) shows Raman spectra of as-grown and purified MWCNTs recorded using an Ar-ion laser at an excitation wavelength of 514.5 nm. The Raman spectrum shows two peaks 1,324.78 and 1,580.73 cm^{-1} typical of the high wave-number region

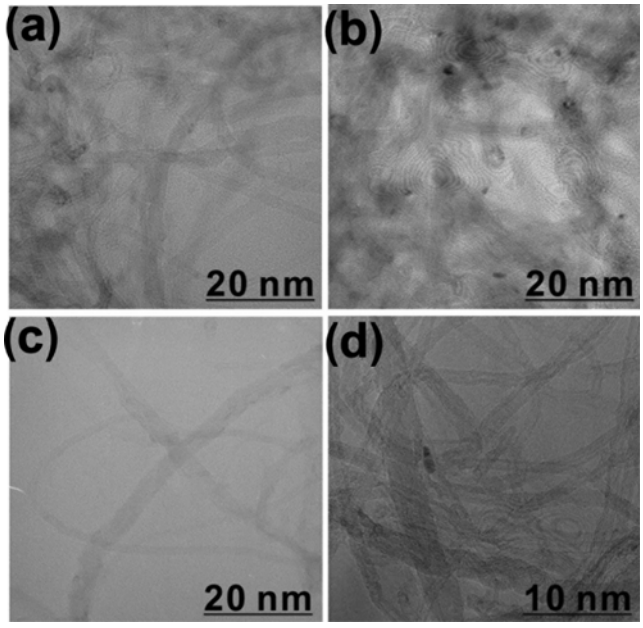

Fig. 4. (a) and (b) are TEM images of as-grown and (c) and (d) pristine MWCNTs prepared over trimetallic catalyst under 10/100 sccm C_2H_2/H_2 flow.

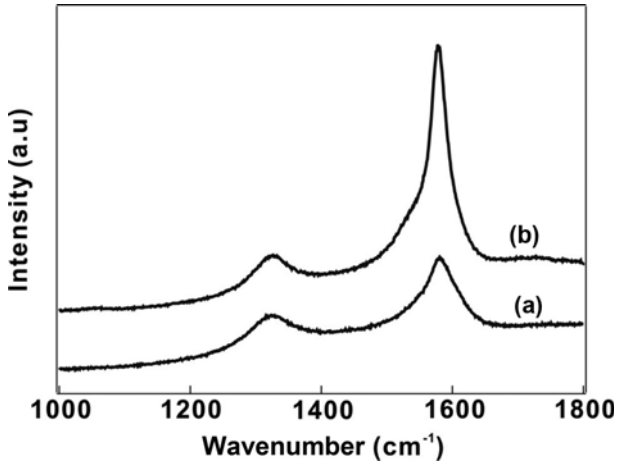

Fig. 5. (a) and (b) are Raman spectra of as-grown and pristine MWCNTs.

of the MWCNTs. These two peaks are related to the disorder-induced (D-band) and tangential graphitized carbon (G-band), respectively [22-24]. The D-band in as-grown is weaker compared to purified MWCNTs and G-band is narrower in the purified MWCNTs compared to as-grown sample. A direct measurement of the D band to G band intensity ratio gives I_D/I_G=0.27 for as-grown MWCNTs, which decreased to 0.12 for pristine MWCNTs, indicating the improvement of the quality of the purified MWCNTs. Another important peculiarity in the Raman spectra of purified MWCNTs is the considerable enhancement of the intensities of the Breit-Wigner-Fano (BWF) shape of lower energy side of the G-band, indicating agglomeration effects that typically occur during acid treatment of as-grown MWCNTs [25].

Nitrogen adsorption isotherms of as-grown and purified MWCNTs are shown in Fig. 6. The profile (a) is a close type II isotherm according to the IUPAC classification [26]. The abrupt rise of as-grown and pristine MWCNTs in the adsorption is attributed to the filling of micropores [27]. The greater accuracy of BET model in fitting the experimental adsorption data, especially at higher pressure is evident in the Fig. 6(b), which contains plot of $1/[V_A(P_O/P-1)]$ vs. P/P_O for all samples. The slope and intercept

Table 1. Comparison of BET SSA of current work with the literature data

Sample ID	Preparation method	Catalyst	NT-Type	Diameter (nm)	BET SSA (m^2/g)	References
CNT-1	CVD	Trimetallic	MWCNTs	4-15	313	[Current]
CNT-2	CVD	Trimetallic	MWCNTs	8-14	647	[Current]
CNT-3	CVD	Bimetallic	MWCNTs	60-80	30	[13]
CNT-4	CVD	Monometallic	MWCNTs	60-80	25	[13]
CNT-5	CVD	Bimetallic	MWCNTs	-	240	[24]
CNT-6	CVD	Bimetallic	MWCNTs	10-20	225	[27]
CNT-7	CVD	Bimetallic	MWCNTs	10-20	349	[27]
CNT-8	CVD	Monometallic	MWCNTs	4-12	376	[28]
CNT-9 (NanoAmor)	CVD	Bimetallic	MWCNTs	10-20	146	[29]
CNT-10 (Timesnano)	CVD	Bimetallic	MWCNTs	10-20	177	[29]
CNT-11 (Mitsui)	CVD	Bimetallic	MWCNTs	40-90	22	[29]
CNT-12 (Timesnano)	CVD	Bimetallic	MWCNTs	10-30	119	[29]
CNT-13 (Timesnano)	CVD	Bimetallic	MWCNTs	10-20	74	[29]
CNT-14 (Timesnano)	CVD	Bimetallic	MWCNTs	20-30	118	[29]
CNT-15 (Timesnano)	CVD	Bimetallic	MWCNTs	10-20	180	[29]
CNT-COOH-16 (Timesnano)	CVD	Bimetallic	MWCNTs	10-20	171	[29]
CNT-OH-17 (Timesnano)	CVD	Bimetallic	MWCNTs	10-20	192	[29]

CVD chemical vapor deposition; NT nanotube; SSA specific surface area. NanoAmor, Timesnano and Mitsui are the companies providing commercial CNTs

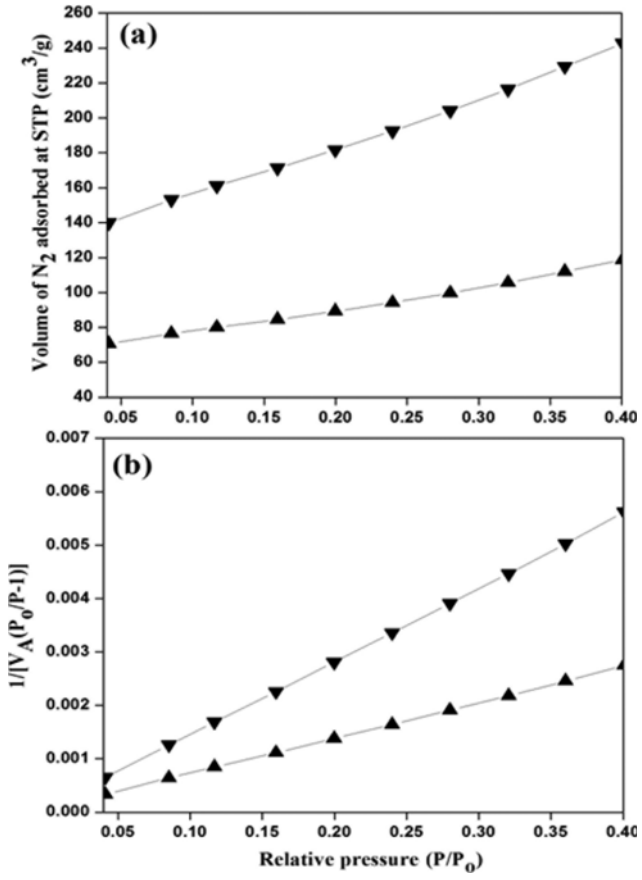

Fig. 6. (a) N_2 adsorption isotherms of as-grown and purified MWCNTs (▲ and ▼) of trimetallic catalyst supported MgO. (b) Plot of $1/V_a[(P_o/P-1)]$ vs P/P_o of as-grown and purified MWCNTs (▼ and ▲) shows linear fit in the relative pressure range of 0-0.4.

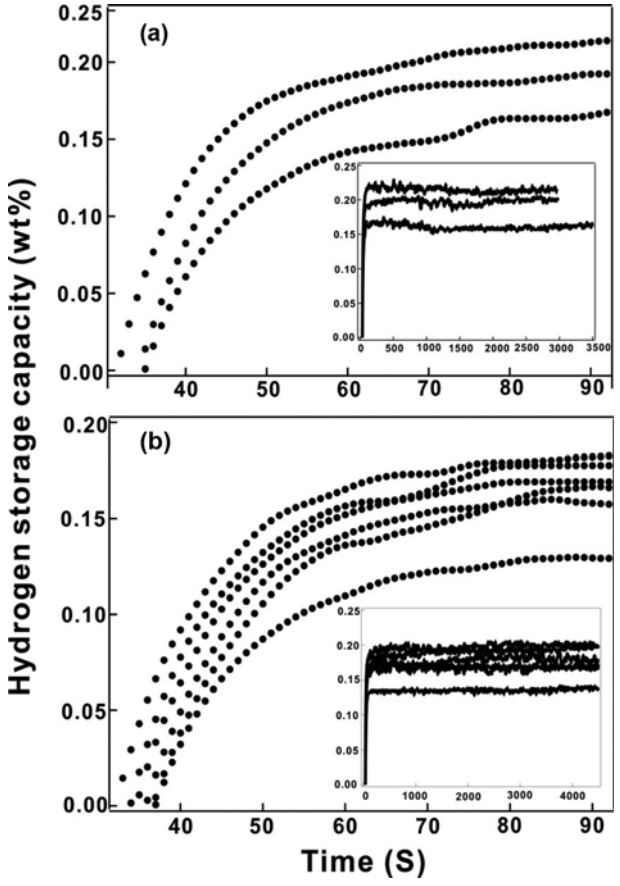

Fig. 7. (a) and (b) are hydrogen storage capacity (wt%) vs time (S) of raw and pristine MWCNTs for a very short time. Inset (a) and (b) is hydrogen storage capacity (wt%) vs time (S) for more than 1 hour after activating at 200 °C.

of these plots are obtained through linear aggression according to the Eq. (1) and are used to compute the BET SSA [26].

$$\frac{1}{n[(P_O/P)-1]} = \frac{i}{cn_m} + \frac{c-1}{cn_m}\frac{P}{P_O} \quad (1)$$

Both CNTs (1-2) prepared in our laboratory and existing CNTs (3-17) shown in Table 1 followed the same experimental conditions [15,26,29-31]. The 313 m^2/g BET-SSA of as-grown MWCNTs increased to 647 m^2/g after purification by 60% HNO_3. The increase in surface area ~294 m^2/g clearly indicates the growth of pristine MWCNTs. Tremendous increase of BET surface area of CNT-1 and CNT-2 samples compared to bimetallic or monometallic catalyst is visible in Table 1. Enormous increase in surface area is due to the purification, which shortened and opened the majority of MWCNTs [28-30]. Trimetallic catalyst has more catalytic activity, selectivity, and stability is also responsible for higher BET SSA. During MWCNT synthesis, high carbon solutbility and diffusion rates are more prominent in Co-Mo-V trimetallic catalyst compared to monometallic and bimetallic and may be also enhancing factor for the improved surface area [32]. Comparison of enhancement of BET SSA of current MWCNTs with the literature BET SSA of MWCNTs prepared via bimetallic and monometallic catalyst is also discussed in Table 1.

The hydrogen storage behavior of MWCNTs at different types of equilibrium pressures is displayed in Fig. 7, where a typical hydrogen storage capacity *vs* time is plotted. The profile (a) and (b) corresponds to hydrogen adsorption of as-grown and purified MWCNTs. The hydrogen storage capacity is ~0.22 wt% for as-grown MWCNTs as shown in Fig. 7(a). The re-adsorption of hydrogen onto the sample previously hydrogenated was performed after outgassing at ambient temperature. The measurement indicated that maximum hydrogen storage capacity of MWCNTs diminished negligibly within the error limit of the measurement. A linear hydrogen storage capacity increase was observed as the equilibrium pressure of as-grown MWCNTs was increased between 1.67 and 1.88 MPa. More than 95% of hydrogen was adsorbed in a very short time (1 min). The inset of Fig. 7(a) displays transient hydrogen storage profiles for the complete duration of the experiment. The maximum hydrogen storage capacity of as-grown MWCNTs was determined using [Wt of H/(Wt of H+Wt of CNTs)]×100 using the Ideal gas equation PV=nRT. Interestingly, hydrogen storage capacity of pristine MWCNTs is ~10% less compared to as-grown MWCNTs performed under similar experimental conditions. The fact is that hydrogen storage capacity increases as the BET surface area increases, but in our case it was not observed

and kinetics of pristine MWCNTs was also less compared to as-grown sample [29]. This suggests that presence of impurities like metals and metal oxides in as-grown sample was responsible for both increased hydrogen storage capacity and fast kinetics. In our synthesized as-grown MWCNTs sample, TGA and EDX show more than 30% impurities such as metals and their oxides. It is well known that transition metals are susceptible to increase the hydrogen storage capacity and kinetics [21,33-35]. Furthermore, enhacement of hydrogen uptake of pristine sample was overshadowed by the presence of metals as impurities in as-grown MWCNTs sample. The readsorption of hydrogen on the hydrogenated pristine sample shows very little variation indicating physisorption of hydrogen on the pristine MWCNTs sample. In Fig. 7(b) the inset shows long time hydrogen storage adsorption on pristine MWCNTs. Pristine MWCNTs also shows linear hydrogen storage capacity increase as the equilibrium pressure of the sample increases between 1.67 and 1.88 MPa.

CONCLUSION

High surface area multi-walled carbon nanotubes have been synthesized by thermal decomposition of acetylene over a new trimetallic catalyst supported MgO. The surface area of as-grown and purified MWCNTs was found to be 313 m^2/g and 643 m^2/g much improved than MWCNTs synthesized by monometallic and bimetallic catalysts. The hydrogen storage capacity of as-grown MWCNTs was ~0.22 wt%, which is ~10% more than pristine MWCNTs (0.20 wt%) activated thermally at 200 °C at equilibrium pressure between 1.68 and 1.88 MPa. The enhanced hydrogen storage capacity and fast kinetics of as-grown samples as compared to pristine was observed due to the presence of impurities such as metals or metal oxides responsible for synthesis of trimetallic catalyst. The fast kinetics and complete reversibility gives the complete indication of physisorption of hydrogen on MWCNTs.

ACKNOWLEDGEMENT

The Author gratefully acknowledges the support of the Department of Chemical and Materials Engineering, King Abdulaziz University.

REFERENCES

1. S. E. Moradi, *Korean J. Chem. Eng.*, **31**(9), 1651 (2014).
2. S. M. A. Ibrahim, *Korean J. Chem. Eng.*, **31**(10), 1792 (2014).
3. J. Yang, A. Sudik, C. Wolverton and D. J. Siegel, *Chem. Soc. Rev.*, **39**, 656 (2010).
4. P. Benard and R. Chahine, *Scripta Mater.*, **56**, 803 (2007).
5. S. M. Lee, K. H. An, Y. H. Lee, G. Seifert and T. Frauenheim, *J Am. Chem. Soc.*, **123**, 5059 (2001).
6. H. M. Cheng, Q. H. Yang and C. Liu, *Carbon*, **39**, 1447 (2001).
7. V. V. Simonyan and J. K. Johnson, *J Alloy. Compd.*, **330-332**, 659 (2002).
8. M. Jorda-Beneyto, F. Suarez-Garcıa, D. Lozano-Castello, D. Cazoria-Amoros and A. Linares-Solano, *Carbon*, **45**, 293 (2007).
9. S. Shi and J. Y. Hwang, *Int. J. Hydrogen Energy*, **32**, 224 (2007).
10. P. Benard, R. Chahine and P. A. Chandonia, *J. Alloy. Compd.*, **446-447**, 380 (2007).
11. L. Zhou, *Renew. Sust. Energy Rev.*, **9**, 395 (2005).
12. Z. Yang, D. M. Grant, P. Wang and G. S. Walker, *Faraday Discuss.*, **151**, 133 (2011).
13. A. C. Dillon and M. J. Heben, *Appl. Phys. A*, **72**, 133 (2001).
14. F. L. Darkrim, P. Malbrunot and G. P. Tartaglia, *Int. J. Hydrogen Energy*, **27**, 193 (2002).
15. N. H. A. Hassan, A. R. Mohamed and S. H. S. Zein, *Diam. Relat. Mater.*, **16**, 1517 (2007).
16. R. Strobel, J. Garche, P. T. Moseley, L. Jorisseh and G. Wolf, *J. Power Sources*, **159**, 781 (2006).
17. Y. Ren and D. L. Price, *Appl. Phys. Lett.*, **79**, 3684 (2007).
18. S. Patchkovskii, J. S. Tse and S. N. Yurchenko, *P. Natl. Acad. Sci. USA*, **102**, 10439 (2005).
19. A. Burian, J. C. Dore and H. E. Fischer, *J. Phys. Rev., B*, **59**, 1665 (1999).
20. P. I. Babaev, M. M. Dubinin and A. A. Isirikyan, *Russ. Chem. B+*, **25**, 1815 (1976).
21. R. Zacharia, K. Y. Kim and A. K. M. F. Kibria, *Chem. Phys. Lett.*, **412**, 369 (2005).
22. A. Jorio, M. A. Pimenta and A. G. S. Filho, *New J. Phys.*, **5**, 139 (2003).
23. N. Melanitis, P. L. Tetlow and C. Galiotis, *J. Mater. Sci.*, **31**, 851 (1996).
24. M. Cinke, J. Li and B. Chen, *Chem. Phys. Lett.*, **365**, 69 (2002).
25. C. Jiang, K. Kempa and J. Zhao, *Phys. Rev. B*, **66**, 161404 (2002).
26. F. Li, Y. Wang, D. Wang and F. Wei, *Carbon*, **42**, 2375 (2004).
27. M. Eswaranoorthy, R. Sen and C. N. R. Rao, *Chem. Phys. Lett.*, **304**, 207 (1999).
28. A. W. Adamson, *Physical Chemistry of Surfaces*, Wiley, NewYork (1990).
29. R. Zacharia, K. Y. Kim and S. W. Hwang, *Catal. Today*, **120**, 426 (2007).
30. D. Y. Kim, C. M. Yang and Y. S. Park, *Chem. Phys. Lett.*, **413**, 135 (2005).
31. M. E. Birch, T. A. Ruda-Eberenz, M. Chai, R. Andrews and R. L. Hatfield, *Ann. Occup. Hyg.*, **57**, 1148 (2013).
32. F. Ding, P. Larsson, J. A. Larsson, R. Ahuja, H. Duan, A. Rosen and K. Bolton, *Nano Lett.*, **8**, 463 (2008).
33. J. Cai, L. Li, X. Lv, C. Yang and X. Zhao, *ACS Appl. Mater. Interfaces*, **6**, 167 (2014).
34. M. Shiraishi, T. Takenobu, A. Yamada, M. Ata and M. Kataura, *Chem. Phys. Lett.*, **358**, 213 (2002).
35. G. G. Wildgoose, C. E. Banks and R. G. Compton, *Small*, **2**, 182 (2006).